



HAL
open science

Modeling of the thermomechanical behavior of rubbers during fatigue tests from infrared measurements

C. Cruanes, Marie-Pierre Deffarges, F. Lacroix, Stéphane Méo

► To cite this version:

C. Cruanes, Marie-Pierre Deffarges, F. Lacroix, Stéphane Méo. Modeling of the thermomechanical behavior of rubbers during fatigue tests from infrared measurements. *International Journal of Fatigue*, 2019, 10.1016/j.ijfatigue.2019.04.035 . hal-02126778

HAL Id: hal-02126778

<https://hal.science/hal-02126778>

Submitted on 22 Oct 2021

HAL is a multi-disciplinary open access archive for the deposit and dissemination of scientific research documents, whether they are published or not. The documents may come from teaching and research institutions in France or abroad, or from public or private research centers.

L'archive ouverte pluridisciplinaire **HAL**, est destinée au dépôt et à la diffusion de documents scientifiques de niveau recherche, publiés ou non, émanant des établissements d'enseignement et de recherche français ou étrangers, des laboratoires publics ou privés.



Distributed under a Creative Commons Attribution - NonCommercial 4.0 International License

Modeling of the thermomechanical behavior of rubbers during fatigue tests from infrared measurements

C. Cruanes^{1*}, M.-P. Deffarges², F. Lacroix² et S. Méo²

¹IMT Lille Douai, Institut Mines-Télécom, Polymers and Composites Technology & Mechanical Engineering Department, F-59500 Douai, France

²Univ. Tours, Univ. Orléans, INSA CVL, LaMé, F-37200 Tours, France

Email : christophe.cruanes@IMT-Lille-Douai.fr

Phone : +0033 2 47 36 12 00

I. Abstract

This paper presents the establishment of an equation fitting the evolution of the self-heating of a polychloroprene rubber (CR) and a natural rubber (NR) during uniaxial fatigue tests. For the CR, dumbbell shaped samples underwent a wide range of loadings was investigated in order to cover low and high cycle fatigue behavior for several load ratios taken between -0.3 and 0.5. The study consists in firstly measuring the evolution of the self-heating during a fatigue test. Then, after computing the derivative, the resulting curve is fit with an equation composed of three components: two of the form of a negative exponential and a constant. It is then integrated to obtain an equation that would fit the evolution of the self-heating for all the loadings investigated. It is observed that the parameters are correlated with the intensity of the stress and the load ratio applied during the test. The same observations were made for the NR on slim samples. Consequently, it is proposed that one of the parameter is linked to the viscosity, the parameter linked to the first negative exponential is related with the viscosity, the parameter linked to the second negative exponential is related to the damage induced by the low cycle fatigue loading and the parameter integrated from the constant is related to the influence of the presence of a sizable crack on the temperature field.

Keywords : Rubber, Fatigue, Thermo-mechanical behavior, LCF/HCF behavior

II. Highlights

- Experimental measurement of the self-heating of Rubbers during fatigue tests
- Thick samples in polychloroprene and slim samples in natural rubber are investigated
- Low and high cycle fatigue, as well as tension-tension and tension-compression, investigated
- Evolution of the self-heating fitted with a double negative exponential law
- Influence of the loading on the parameters of the equation highlights the LCF/HCF limit
- The parameters of the equation are proposed to be linked with mechanical properties of the rubber

III. Literature

Rubbers are widely used in the industry thanks to their ability to undergo large strain and to dampen energy. Consequently, they do not evacuate heat easily, meaning that the temperature of a rubbery part can reach significant levels, impacting its mechanical behavior. This is an issue that needs to be anticipated.

One consequence is that rubbers can exhibit self-heating under a mechanical loading without undergoing noticeable damage [Honorat 2006; Wattrisse et al. 2011] which is mainly caused by the viscoelasticity property of those materials [Medalia 1991; Meinecke 1991]. The latter depends on the strain rate [Lion 1997], the maximum loading [harbour et al. 2008; Cruanes et al. 2013] and the shape of the sample [Ayoub et al. 2012]. Moreover, under suitable conditions and depending of the type of rubber, the Strain Induced Crystallization (SIC) can be detected by a change in the evolution of the self-heating. However, the influence of the SiC is better observed when working on the thermal sources [Samaca Martinez et al. 2013].

The thermo-mechanical behavior of rubbers during fatigue tests has also been investigated. In some cases, the modeling of the evolution of the self-heating was the target: [Boukamel et al. 2001] have proposed a solution for the thermo-mechanical problem using a variational formulation applied on the rheological model of Poynting–Thomson. The later implementation into a FE code achieved its numerical solution [Meo et al. 2002]. Another approach from [Ovalle Rodas et al. 2014] was to develop a large strain thermoviscoelastic constitutive model to describe the self-heating of rubber material Low Fatigue Life tests. [Lejeunes et al. 2018] pushed it forward to describe the chemico-mechanical behavior of rubber.

In other case a 0D approach was considered as a way to anticipate the fatigue life when coupled with another technique [Le Saux et al. 2010a; Marco et al. 2017]. The thermal measurement would also allow for a rapid determination of the transition between Low Cycle (LCF) and High Cycle Fatigue (HCF) behaviors (figure 1 [Cruanes et al. 2014; Le Saux et al. 2010b]). This method applied on rubbers was initially developed from studies on other materials (metals on the figure 2 [Luong 1998; La Rosa et Risitano 2000; Doudard et al. 2005] or short fiber reinforced polymers [Jegou et al. 2013]).

In this article, an experimental thermo-mechanical model based on the evolution of the self-heating of a polychloroprene rubber and a natural rubber during a fatigue test is proposed.

IV. Experimental set up

a. Material and sample

The first material studied is a vulcanized polychloroprene rubber (CR) filled with N990 carbon black (Table 1). The specimen used were dumbbell-shaped (Figure 3 – volume around 4500mm³) made of a rubber part 30 mm long, bounded at each extremity with two metal grip parts, subsequently

attached to the fatigue machine with screws. Those specimens were injection molded at 175°C for 4 minutes.

The second material is a vulcanized natural rubber (NR) filled with carbon black. The specimen used is rectangular shaped (30x10x2mm – volume around 600mm³) (Table 2). It was cut from a plate injection molded at 160°C.

b. Machines and loading

i. Fatigue tests

1. Polychloroprene rubber

The fatigue tests for the CR samples were conducted on a servo-hydraulic fatigue testing machine INSTRON 8802 at room temperature. They consisted in uniaxial force-controlled tests with a sinusoidal signal at a frequency of 5Hz.

The loadings investigated are detailed in the Table 3. They allowed the differentiation between both Low and High Fatigue Life behaviors. The load ratio ($R = \frac{\sigma_{min}}{\sigma_{max}}$) sweeps from -0.3 to 0.5 as it has shown to significantly influence the fatigue behavior of the CR [Poisson et al. 2012; Mars 2008]: the increase of the load ratio would show an enhancement of the fatigue life explained by the Strain Induced Crystallization being more significant. The amplitude stress sweeps across the Low and High Cycle fatigue tests for each load ratio. For each loading, two or three samples were tested.

2. Natural rubber

The fatigue tests for the NR samples were conducted on an Electroforce BOSE 3300 at room temperature. They consisted in uniaxial displacement-controlled tests with a sinusoidal signal at a frequency of 5Hz at a 0.2 load ratio. 4 samples were used for each loading at the same time. The loadings were chosen so that at least one test would be lower than the LCF/HCF limit (Figure 4). The amplitude strains investigated are 20%; 30%; 50% and 66%.

ii. Infrared thermography

The thermal measurements have been conducted with an infrared camera CEDIP Jade III MWIR (InSb) at an acquisition frequency of 50Hz. The focal plane array is a 320x240 array of detectors digitized on 14 bits and sensitive in the 3.6 – 5.1μm spectral band wave-lengths. Before the campaign, a calibration was realized to check the conversion of the signal into temperature (in °C). In order to do that, a black body was used and a 2 points Non Uniformity Correction (NUC) was applied to the array of detectors. After calibration, a 25 mK precision was obtained. To minimize the influence of the external environment on the measurement, a black sheet was placed around the fatigue machine.

Three areas were measured in order to obtain the self-heating of the sample (Figure 5): the two grips (boxes 2 and 3) and the main area (box 1). In each box, the maximum temperature was measured and then the self-heating was calculated following the equation at a given time:

$$\theta = \max(T_1) - \frac{\max(T_2) + \max(T_3)}{2}$$

Where $\max(T_1)$ is the maximum temperature measured in the box 1 around the main area, $\max(T_2)$ (respectively $\max(T_3)$) is the maximum temperature measured in the box 2 on the top grip (resp. in the box 3 on the bottom grip). The self-heating at the beginning of the test depends on the temperature of the grips. It is considered in this paper that the initial self-heating is equal to 0°C.

V. Model

a. Specific durations

Beforehand, two durations are defined in order to be integrated in the model.

Firstly, N_s is the number of cycles for which the self-heating describes an inflection point. It was observed to be around 1000 cycles for all the investigated loadings (Figure 6).

Secondly, N_θ is the number of cycles from which the derivative of the self-heating is for the first time during test lower than 10^{-4} °C/cycles (Figure 7). From this point on, the derivative was considered stabilized.

b. Establishing the equation of the self-heating

Once those durations defined, it is proposed that the derivative of the evolution of the self-heating, depicted on the Figure 8, could be fit with an equation given by:

$$\frac{d\theta}{dN} = A_1 e^{-\frac{N}{\tau_1}} + A_2 e^{-\frac{N}{\tau_2}} + \dot{\theta}_L \quad (1)$$

With $\dot{\theta}_L$ being the value toward which the self-heating derivative tends to, A_1 and A_2 being constants (in °C/cycle). τ_1 and τ_2 are also constants (in number of cycles) and they will be used to fit the evolution of the self-heating.

Therefore, the integrated form corresponding to the evolution of the self-heating itself would be as follow:

$$\theta(N) = -A_1 \tau_1 e^{-\frac{N}{\tau_1}} - A_2 \tau_2 e^{-\frac{N}{\tau_2}} + \dot{\theta}_L \cdot N + \gamma \quad (2)$$

With γ being a constant resulting from the integration.

Three boundary conditions are defined in order to calculate the constants A_1 , A_2 and γ :

a- $\frac{d\theta}{dN}(N = 0) = \dot{\theta}_0$

b- $\theta(N = 0) = \theta_0$

c- $\frac{d\theta}{dN}(N = N_s) = \dot{\theta}_N$

The condition (c) corresponds to the heating rate as described in [Cruanes et al. 2013; Cruanes et al. 2014]. From those articles, the heating rate is strongly linked with the loading and therefore can be considered as a characteristic parameter for the given fatigue test.

Then it comes by identification that the constants of the equation are:

$$\gamma = A_1\tau_1 + A_2\tau_2 + \theta_0 \quad (3)$$

$$A_1 = \frac{\dot{\theta}_0 e^{\frac{-N_s}{\tau_2}} - \dot{\theta}_N + \dot{\theta}_L \left(1 - e^{\frac{-N_s}{\tau_2}}\right)}{e^{\frac{-N_s}{\tau_2}} - e^{\frac{-N_s}{\tau_1}}} \quad (4)$$

$$A_2 = \frac{-\dot{\theta}_0 e^{\frac{-N_s}{\tau_1}} + \dot{\theta}_N - \dot{\theta}_L \left(1 - e^{\frac{-N_s}{\tau_1}}\right)}{e^{\frac{-N_s}{\tau_2}} - e^{\frac{-N_s}{\tau_1}}} \quad (5)$$

It gives the final form:

$$\theta(N) = A_1\tau_1 \left(1 - e^{\frac{-N}{\tau_1}}\right) + A_2\tau_2 \left(1 - e^{\frac{-N}{\tau_2}}\right) + \dot{\theta}_L \cdot N + \theta_0 \quad (6)$$

The Figure 9.a shows that it fits well with the experimental evolution of the self-heating of the dumbbell in polychloroprene for all the investigated loadings at a load ratio of 0.1 (one test per loading, for the sake of clarity). The tests undergoing an amplitude stress lower or equal to 0.44MPa are in the HCF area, consequently the others are in the LCF (Figure 1). The Figure 9.b shows that the equation (6) fits also well for the slim samples in natural rubber. The tests at an amplitude strain of 20% are below the LCF/HCF limit while the other tests are in the LCF area. It appears that this equation looks like a more complicated version of what is used on the metals or composites [Krapez et al. 2000; Crupi 2008, Jegou et al. 2013]. Indeed, for those materials the equation describing the evolution of the self-heating was found to be [Crupi et al. 2015]:

$$\theta(N) = K \cdot N^* \left(1 - e^{\frac{-N}{\tau}}\right) \text{ with } \tau = 1.5N^* \quad (7)$$

With K being expressed as a function of several material parameters such as the load conditions and N^* being the number of cycles where the evolution of the self-heating exhibits the transition between the first (transient evolution) and the second phase (stabilized evolution).

VI. Results

a. Definition of normalized parameters

i. Normalized alternate stress

The normalized alternate stress $\sigma_{a,n}$ is defined as:

$$\sigma_{a,n} = \frac{\sigma_a}{\sigma_{a,lim}}$$

Where $\sigma_{a,lim}$ is the limit between Low and High Cycle Fatigue behaviors [Cruanes et al. 2014, Cruanes 2015] as indicated on the Figure 1.

ii. Normalized parameters of the equation

A normalized parameter is needed to show their relative weight in the equation (6).

The parameter $A_i\tau_i^s$ is defined as:

$$A_i\tau_i^s = \frac{|A_i\tau_i|}{|A_1\tau_1|+|A_2\tau_2|+|\dot{\theta}_L N_\theta|} \quad (8)$$

Where $A_i\tau_i$ can be $A_1\tau_1$, $A_2\tau_2$ or $\dot{\theta}_L N_\theta$.

The parameters $A_1\tau_1$ and $A_2\tau_2$ are found in the equation (6) and so is $\dot{\theta}_L \cdot N$. However, the latter is not a constant and cannot be compared to the two other parameters. To do so, it was decided to set the number of cycles N equal to N_θ , the number of cycles from which the derivative is constant.

b. Evolution of τ_i , A_i or $A_i\tau_i$

The parameters $(\tau_1 ; \tau_2)$ showed to be more scattered than the $(A_1\tau_1 ; A_2\tau_2)$: it can be explained by the fact that $(A_1 ; A_2)$ are not only a function of the $(\tau_1 ; \tau_2)$ but also of $\dot{\theta}_0$, θ_0 , $\dot{\theta}_N$ and N_s .

This is why only the $(A_1\tau_1 ; A_2\tau_2)$ is investigated.

c. Each load ratio taken separately

For the dumbbell samples in polychloroprene, the evolution of the parameters $A_i\tau_i$ is followed as they represent the weight of each member of the equation (6). The results depicted in this paragraph are given for R=0.1. It is important to note that for the other load ratios, this investigation lead to the same observations.

The Figure 01 shows the evolution for $A_1\tau_1$, $A_2\tau_2$, $\dot{\theta}_L N_\theta$ and for their sum versus the normalized amplitude stress (for R=0.1).

Several remarks should be given from the Figure 10:

- The overall sum of the $A_i\tau_i$ is steadily increasing with the loading.
- Each $A_1\tau_1$ increases with the loading, although slightly slows down for the higher loadings.
- The $A_2\tau_2$ is non-significant for the lower loading and increases for the higher loadings.
- The $\dot{\theta}_L N_\theta$ remains very low whatever the test conditions.

The figure 11 shows the evolution of the normalized $A_i\tau_i^s$ versus the normalized amplitude stress at R=0.1.

$A_1\tau_1^S$ and $A_2\tau_2^S$ show the same change of behavior. Firstly the evolution is constant ($A_1\tau_1^S \approx 1$ and $A_2\tau_2^S \approx 0$). Then, for the same normalized amplitude stress, both $A_i\tau_i^S$ exhibit a change of behavior being followed by a linear evolution.

The slim samples in natural rubber show the same results (Figure 12) with the limit LCF/HCF being between 20% and 30%.

$\dot{\theta}_L N_\theta^S$ remains very low throughout the test with a small increase for the highest loadings but it fails to be relevant compared to the other two parameters.

d. Polychloroprene – All load ratios

The evolution of $A_1\tau_1^S$ (respectively $A_2\tau_2^S$) with the normalized amplitude stress for all the load ratios is depicted on the Figure 13 (resp. Figure 14). For the sake of clarity, only the averaged values for a given normalized load ratio are plotted. The evolution of the $\dot{\theta}_L N_\theta^S$ is not considered in this paragraph as the values are marginal compared to the other two parameters.

In the Figure 13, $A_1\tau_1^S$ depicts, for each load ratio, two behaviors: for the lower loadings, it remains close to 1, and from the normalized amplitude stress higher than a value around 1, $A_1\tau_1^S$ steadily decreases.

In the Figure 14, $A_2\tau_2^S$ displays a change of evolution for the normalized amplitude stress as $A_1\tau_1^S$, going from almost 0 to a steady increase.

For both parameters, it is possible to assort the load ratios as follows: the load ratios lower or equal to 0, the 0.1 and 0.2 load ratios and finally those higher than 0.3. Those three groups exhibit similar behavior with two main differences:

- The value of the normalized amplitude stress (from which the $A_i\tau_i^S$ change their behavior) differs according to the group: for load ratios lower than 0 the change occurs around 0.96, while it is around 1.05 for 0.1 and 0.2 and around 1.1 for higher load ratios.
- The slope of the linear variation for the higher loadings is the same for the load ratios lower than 0. For load ratios higher, it decreases when the load ratio increases.

One explanation of such a load ratio driven behavior could be the influence of the Strain Induced Crystallization ([Mars 2008]) as it can be paralleled with the observations given by [Poisson et al. 2011] for the same material (Figure 15).

VII. Analysis

In this part, a physical meaning for the parameters of the equation (6) is proposed.

$$\theta(N) = A_1\tau_1 \left(1 - e^{-\frac{N}{\tau_1}}\right) + A_2\tau_2 \left(1 - e^{-\frac{N}{\tau_2}}\right) + \dot{\theta}_L \cdot N + \theta_0 \quad (6)$$

The equation (6) is decomposed in four terms. While θ_0 can be seen as a constant taking into account the small difference of temperature between the sample's and the ambient's at the beginning of the test, the three other terms are proposed to have the physical meaning described in this part.

$A_1\tau_1$:

The $A_1\tau_1$ is vastly dominant compared to the other terms for the loadings in the High Cycle Fatigue phase. In the Low Cycle Fatigue phase, its contribution in the self-heating of the sample steadily decreases with the increase of the load. However, the Figure 10 shows that the evolution of $A_1\tau_1$ versus the loading slightly slows down while both the $A_2\tau_2$ (mostly) and the $\dot{\theta}_L N_\theta$ (significantly) increase in the LCF phase.

Therefore, $A_1\tau_1$ could be related to the viscosity of the rubber.

$A_2\tau_2$:

For the $A_2\tau_2$, it seems to become relevant from a load measured as the LCF/HCF limit suggesting a correlation between a short duration test (thus more damaging for the sample) and an increase of the $A_2\tau_2$. This could be a consequence of the damage undergone by the sample. In [Cruanes et al. 2016], the porosity of the sample would increase throughout a severe loading fatigue test. This increase was found to be caused mainly by the increasing number of micro-cracks, depicting a widespread damage in the sample [Cruanes 2015; Huneau et al. 2016].

Therefore, $A_2\tau_2$ could stand for the weight of widespread damage on the self-heating.

$\dot{\theta}_L N_\theta$:

The $\dot{\theta}_L N_\theta$ is proposed to be a depiction of the influence of the located damage (such as macro-cracks) on the self-heating: it reached to low values compared to the other two parameters. It is most likely due to the massive volume of the bulk sample and the lesser influence of the macro-cracks of the self-heating. Indeed, the Figure 16 shows a comparison between the influence on the self-heating associated with the presence of a macro crack on a cylindrical sample (from this study) and a slim dumbbell sample (in NR) [Kerchman et Shaw, 2003]: it appears that the impact of the crack in the first case (in the circled area on the Figure 16.a) is not as significant as in the second case (Figure 16.b).

Conclusion

This paper proposed to fit experimental measurements of the self-heating of dumbbells in poly chloroprene rubber and slim samples in natural rubber during fatigue tests with an experimental thermo-mechanical law. It was based on the analysis of the evolution of the self-heating derivative. The integration would lead to an equation describing the evolution of the self-heating. The law would show a very good fit, independently of the shape of the sample (large or small volume).

It would be then proposed to link the parameters of this equation to different physical phenomena involved in the fatigue behavior of this material through observations about their evolutions versus the normalized amplitude stress. Therefore, the $A_1\tau_1$ would be caused by the viscosity, the $A_2\tau_2$ would be caused by the widespread damage and the $\dot{\theta}_L N_\theta$ would be caused by the localized damage (macro-cracks).

Acknowledgment

The authors would like to thank M. Venin from the CERMEL (Tours) for his invaluable help.

References

- [Honorat 2006] Honorat V., PhD Thesis, **2006**, *Université de Montpellier II*
- [Wattrisse et al. 2011] B. Wattrisse, R. Caborgan, J.-M. Muracciole, L. Sabatier, A. Chrysochoos. Dissipative and coupling effects accompanying the natural rubber elongation. *SEM2011*, Jun **2011**, Uncasville, United States.
- [Medalia 1991] Medalia A., *Rubber Chemistry and Technology*, **1991**, 64, 481 – 492
- [Meinecke 1991] Meinecke E., *Rubber Chemistry and Technology*, **1991**, 64, 269 – 284
- [Lion 1997] Lion A. , On the large deformation behavior of reinforced rubber at different temperatures. *Journal of the Mechanics and Physics of Solids*, **1997**, 45;1805–1834.
- [Harbour et al. 2008] Harbour R.J., Fatemi A., Mars W.V., Fatigue crack growth of filled rubber under constant and variable amplitude loading conditions, *Fatigue and fracture of engineering materials structures*, **2007**, 30:640-652
- [Cruanes et al. 2013] C Cruanes, G Berton, F Lacroix, JL Poisson, S Méo, N Ranganathan, Study of fatigue behavior of rubber like materials with infrared thermography methods, *Constitutive Models for Rubber VIII*, **2013**
- [Ayoub et al. 2012] Ayoub, G., Naït-Abdelaziz, M., Zaïri, F., Gloaguen, J.M., Charrier, P., Fatigue life prediction of rubber-like materials under multiaxial loading using a continuum damage mechanics approach: effects of two-blocks loading and R ratio. *Mechanics of Materials*, **2012**, 52: 87–102.
- [Samaca Martinez et al. 2013] Samaca Martinez J.R., Le Cam J.B., Balandraud X., Toussaint E., Caillard J., Mechanisms of deformation in crystallizable natural rubber. Part 1: Thermal characterization, *Polymer*, **2013**, 54: 2717-2726
- [Boukamel et al. 2001] Boukamel A. , Méo S., Débordes O., Jaeger M., A thermo-viscoelastic model for elastomeric behavior and its numerical application. *Archive of Applied Mechanics*, **2001**, 71;785–801.
- [Meo et al. 2002] Meo S., Boukamel A., Debordes O., An alysis of a thermoviscoelastic model in large strain. *Computers and Structures*, **2002**, 80; 2085–2098.
- [Ovalle Rodas et al. 2014] Ovalle Rodas C., Zaïri F., Naït-Abdelaziz M., A finite strain thermo-viscoelastic constitutive model to describe the self-heating in elastomeric materials during low-cycle fatigue, *Journal of the Mechanics and Physics of Solids*, **2014**, 64:396-410

- [Lejeunes et al. 2018] Lejeunes S., Eyheramendy D., Boukamel A., Delattre A., Méo S., Dela Aho K., A constitutive multiphysics modeling for nearly incompressible dissipative materials: application to thermo-chemo-mechanical aging of rubbers, *Mechanics of Time-Dependent Materials, Society for Experimental Mechanics*, **2018**, 22:51-66
- [Le Saux et al. 2010a] Le Saux V., Marco Y., Calloch S., Doudard C., Charrier P., An energetic criterion for the fatigue of rubbers: an approach based on a heat build-up protocol and μ -tomography measurements, *Procedia Engineering*, **2010**, 2:949-958
- [Marco et al. 2017] Marco Y., Huneau B., Masquelier I., Le Saux V., Charrier P., Prediction of fatigue properties of natural rubber based on the descriptions of the cracks population and of the dissipated energy, *Polymer Testing*, **2017**, 59:67-74
- [Cruanes et al. 2014] Cruanes C., Berton G., Lacroix F., Méo S., Ranganathan N., Study of the fatigue behaviour of the polychloroprene rubber for uniaxial tests with infrared methods, *Elastomery*, **2014**, 18:3-9
- [Le Saux et al. 2010b] Le Saux V., Marco Y., Calloch S., Doudard C., Charrier P., Fast evaluation of the fatigue lifetime of rubber-like materials based on a heat build-up protocol and micro-tomography measurements, *International Journal of Fatigue*, **2010**, 32:1582-1590
- [Luong 1998] Luong M.P., Fatigue limit evaluation of metals using an infrared thermographic technique, *Mechanics of Materials*, **1998**, 28:155-163
- [La Rosa et Risitano 2000] La Rosa G. et Risitano A., Thermographic methodology for rapid determination of the fatigue limit of materials and mechanical components, *International Journal of Fatigue*, **2000**, 22, 65 – 73
- [Doudard et al. 2005] DOUDARD C., CALLOCH S., CUGY P., GALTIER A. and HILD F., A probabilistic two-scale model for high-cycle fatigue life predictions, *Fract Engng Mater Struct*, **2005**, 28:279-288
- [Jegou et al. 2013] Jegou L., Marco Y., Le Saux V. et Calloch S., Fast prediction of the Wöhler curve from heat build-up measurements on Short Fiber Reinforced Plastic, *International Journal of Fatigue*, **2013**, 47, 256 –267
- [Le Gac et al. 2018] Le Gac P.-Y., Albouy P.-A., Petermann D., Strain-induced crystallization in an unfilled polychloroprene rubber: Kinetics and mechanical cycling, *Polymer*, **2018**, 142:209-217
- [Zhang et al. 2011] Zhang P., Huang G., Qu L., Nie Y. Weng G., Wu J., Strain-Induced Crystallization Behavior of Polychloroprene Rubber, *Journal of Applied Polymer Science*, **2011**, 121, 37 – 42
- [Crupi et al. 2008] Crupi V., An unifying approach to assess the structural strength, *International Journal of Fatigue*, **2008**, 30, 1150-1159
- [Krapez et al. 2000] Krapez J., Pacou D., Gardette G., Lock-in thermography and fatigue limit of metals, *OFFICE NATIONAL D ETUDES ET DE RECHERCHES AEROSPATIALES ONERA-PUBLICATIONS-TP*, **2000**.
- [Crupi et al. 2015] Crupi V., Guglielmino E., Risitano G., Tavilla F., Experimental analyses of SFRP material under static and fatigue loading by means of thermographic and DIC techniques, *Composites Part B*, **2015**, 77, 268-277
- [Poisson et al. 2011] Poisson J.-L., Lacroix F., Meo S., Berton G. et Ranganthan N., Biaxial fatigue behavior of a polychloroprene rubber, *International Journal of Fatigue*, **2011**, 33, 1151 – 1157
- [Mars 2008] Mars W.V., COMPUTED DEPENDENCE OF RUBBER'S FATIGUE BEHAVIOR ON STRAIN CRYSTALLIZATION, *Rubber Chemistry and Technology*, **2008**, 82:51-61]
- [Cruanes et al. 2016] Cruanes C., Lacroix F., Berton G., Méo S., Ranganathan N., Study of the fatigue behavior of a synthetic rubber undergoing cumulative damage tests, *International Journal of Fatigue*, **2016**, 91:322-327

[Cruanes 2015] Cruanes C., PhD Thesis, **2015**, *Université de Tours*

[Huneau et al. 2016] Huneau B., Masquelier I., Marco Y., le Saux V., Noizet S., Schiel C. et Charrier P., Fatigue crack initiation in a carbon black-filled natural rubber, *Rubber Chemistry and Technology*, **2016**, 89:126–141

[Kerchman et Shaw. 2003] Kerchman V., Shaw C., EXPERIMENTAL STUDY AND FINITE ELEMENT SIMULATION OF HEAT BUILD-UP IN RUBBER COMPOUNDS WITH APPLICATION TO FRACTURE, *Rubber Chemistry and Technology*, **2003**, 76:386-405

Elastomer	Polychloroprene
Filler	Carbon black (N990)
Curative system	S-ZnO-MgO

Table 1 – Main components present in the polychloroprene rubber used in this study

Elastomer	Natural Rubber
Filler	Carbon black
Curative system	S-ZnO-PPD

Table 2 – Main components present in the natural rubber used in this study

AMPLITUDE STRESS (MPa)								
R	Load 1	Load 2	Load 3	Load 4	Load 5	Load 6	Load 7	Load 8
-0.3	0.552	0.634	0.689	0.772	0.827	0.882	0.965	
-0.1	0.467	0.537	0.583	0.653	0.700	0.747	0.817	
0	0.361	0.424	0.488	0.530	0.594	0.636	0.679	0.742
0.1	0.325	0.382	0.439	0.477	0.535	0.573	0.611	0.668
0.2	0.390	0.424	0.475	0.509	0.543	0.594		
0.3	0.371	0.416	0.445	0.475	0.520			
0.5	0.265	0.297	0.318	0.339	0.371	0.403	0.445	

Table 3 – Loads investigated during the fatigue testing campaign.

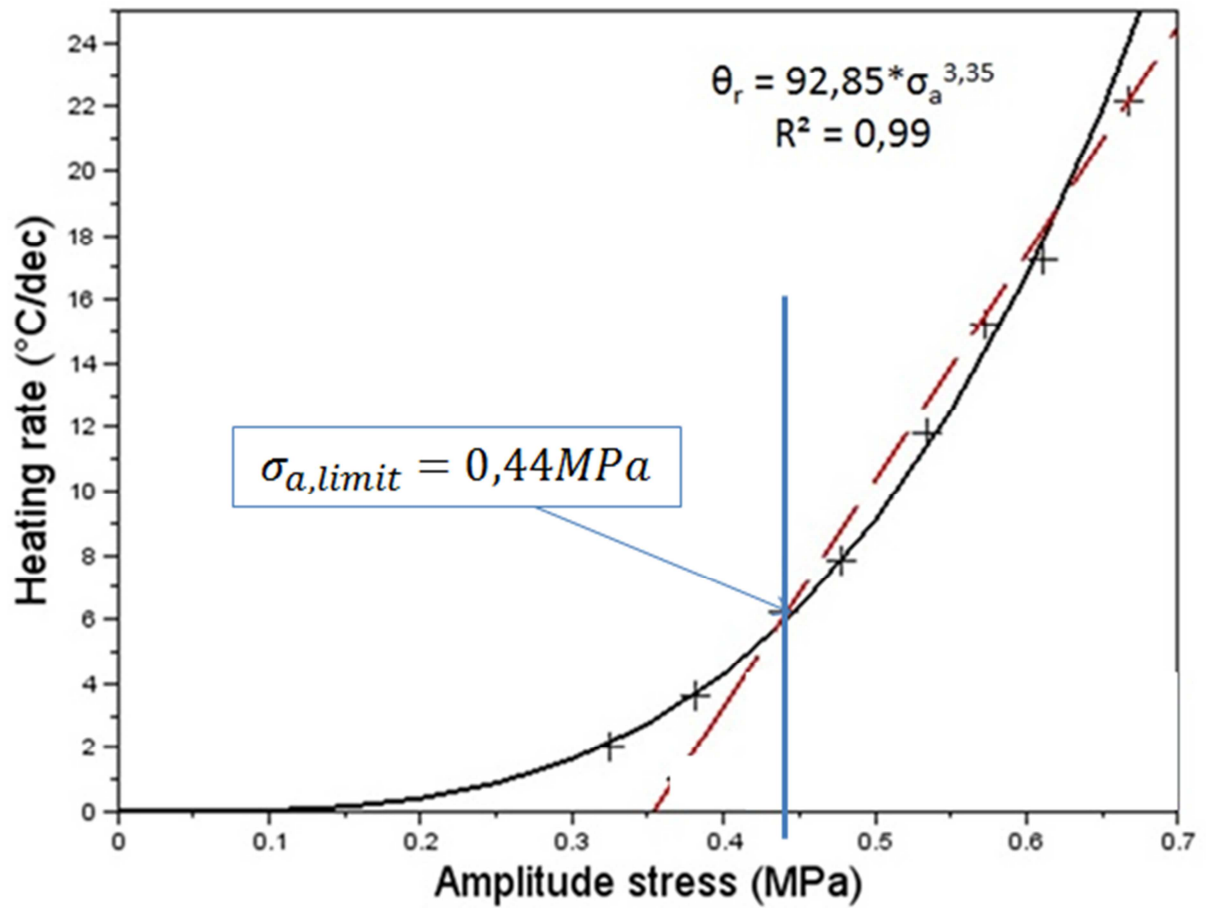


Figure 1 – Measurement of the LCF/HCF limit for a polychloroprene rubber with the rapid method (from [Cruanes et al. 2014])

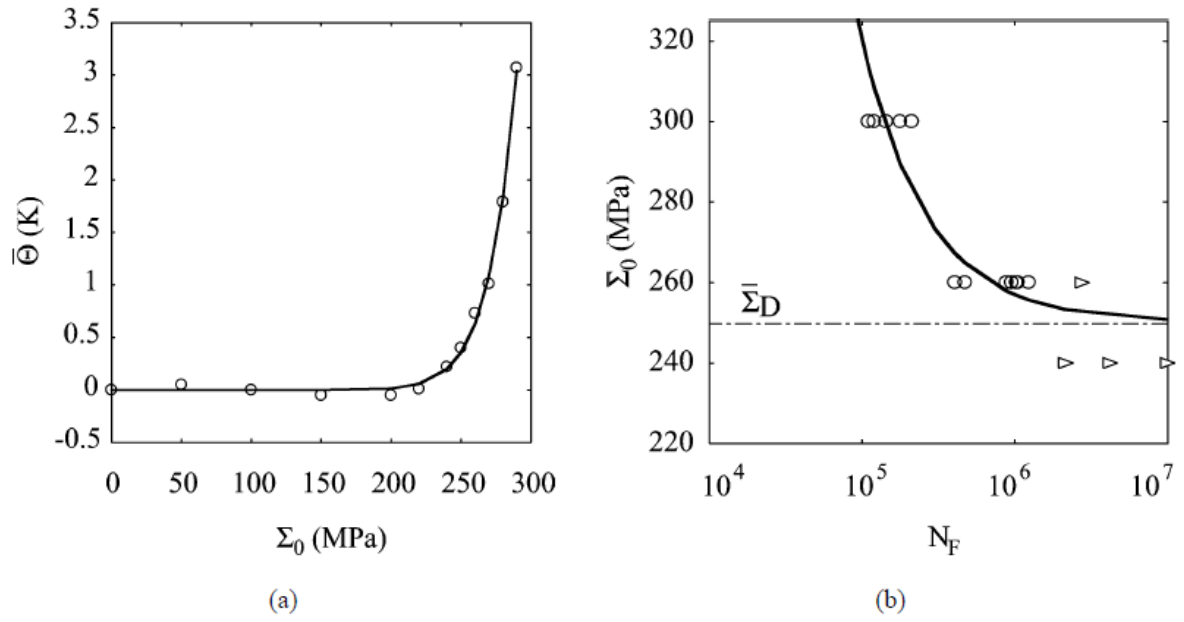


Figure 2 – Taken from [Doudard et al. 2005]: a/ Evolution of the self-heating versus the applied stress and b/ the Wöhler curve for the given tests.

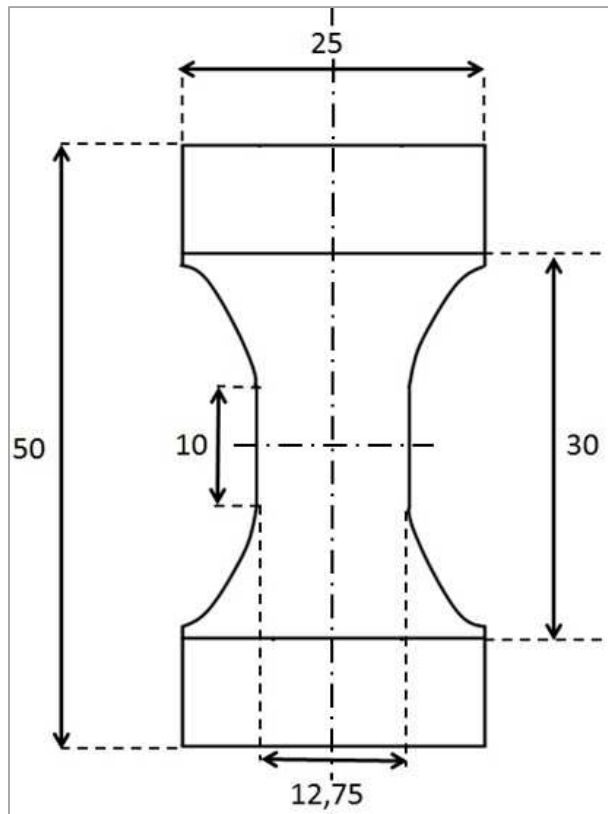


Figure 3 – Shape and dimensions (in millimeters) of the sample used

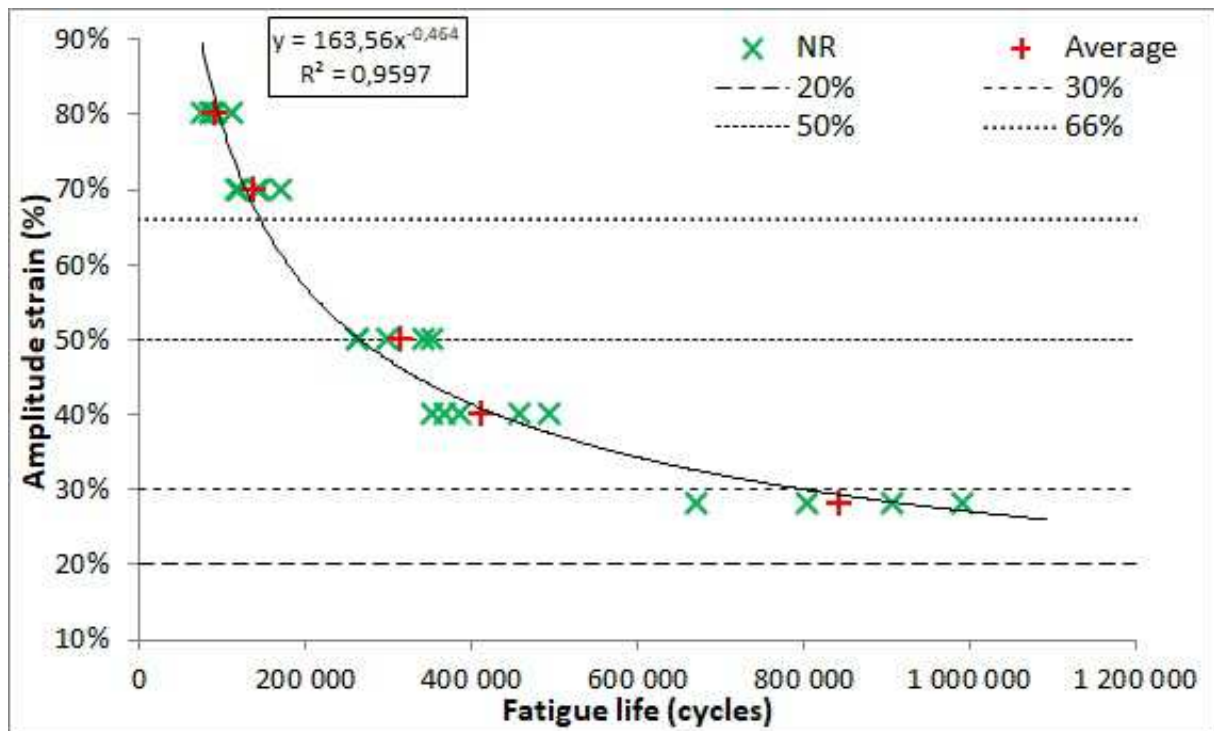


Figure 4 – Wöhler curve for the natural rubber

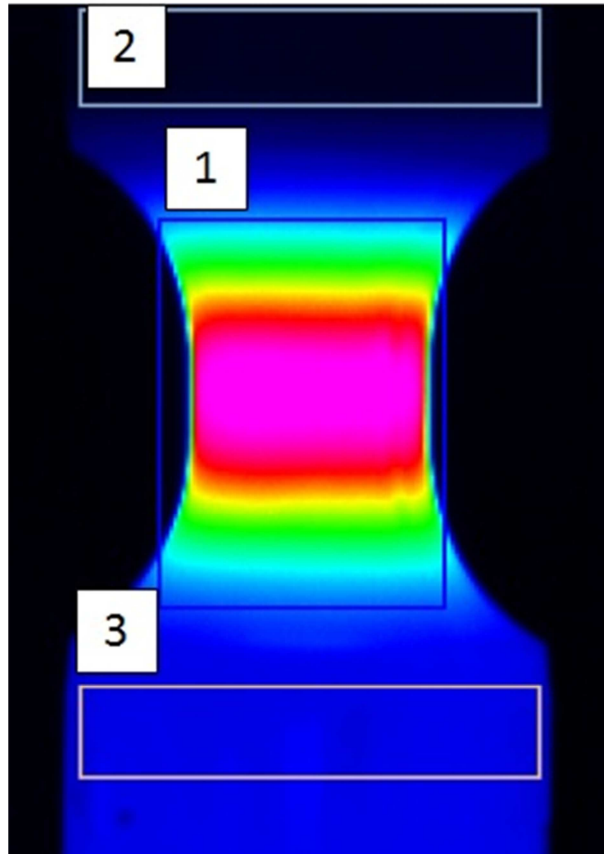


Figure 5 – Measurement of the temperatures at the surface of the main area (box 1), top (box 2) and bottom grip (box 3).

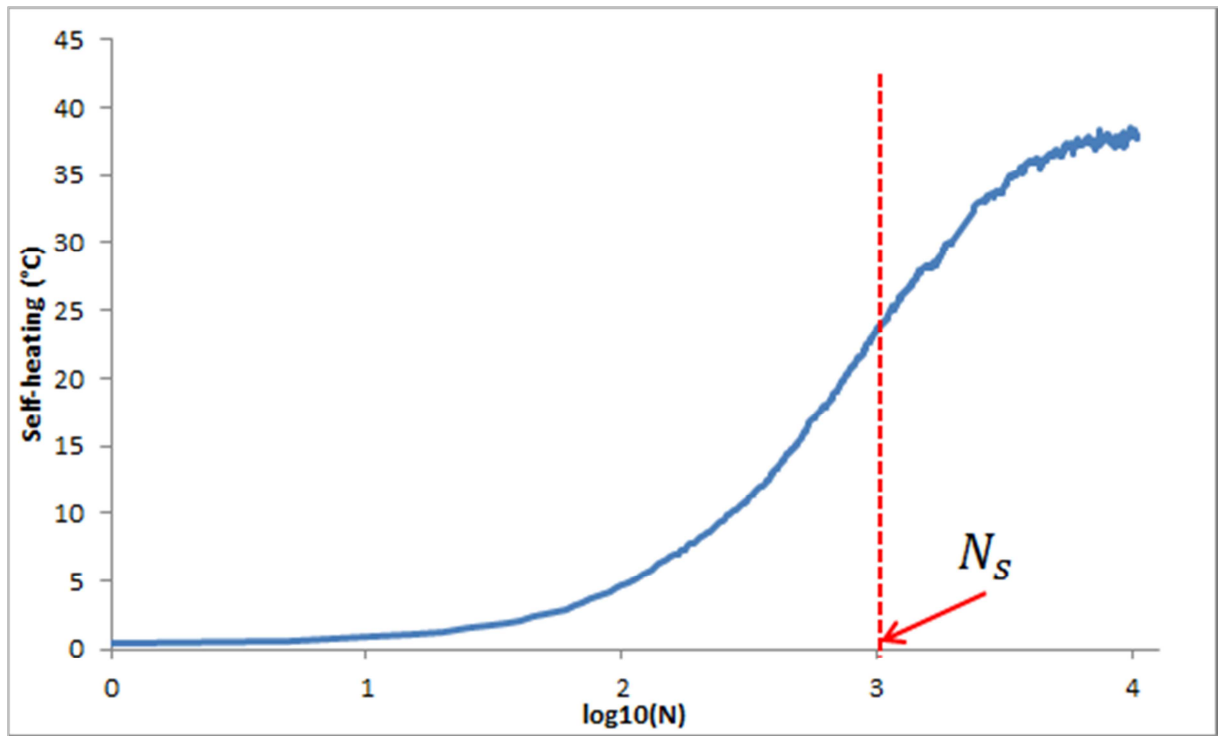


Figure 6 – Evolution of the self-heating during a fatigue test (R=0.1, Maximum load = 175N and fatigue life = 10^4 cycles).

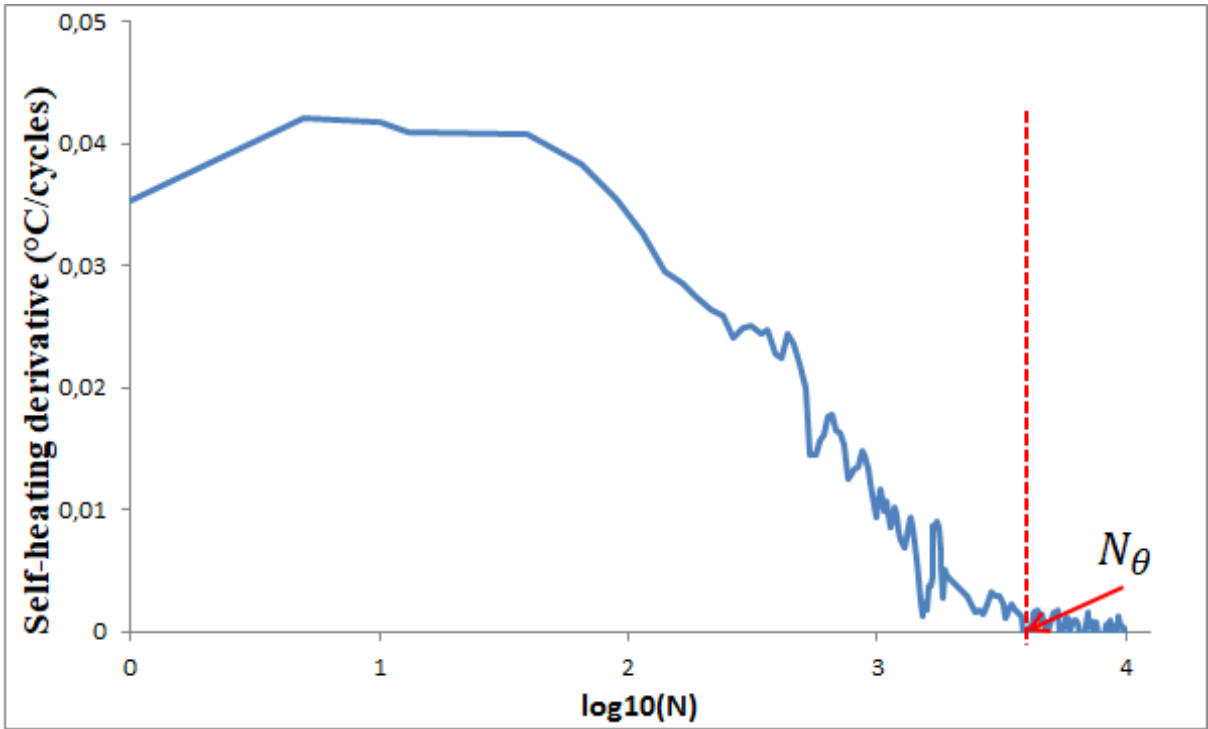


Figure 7 – Evolution of the self-heating derivative during a fatigue test in the same conditions as on the figure 5 (R=0.1, Maximum load = 175N and fatigue life = 10^4 cycles).

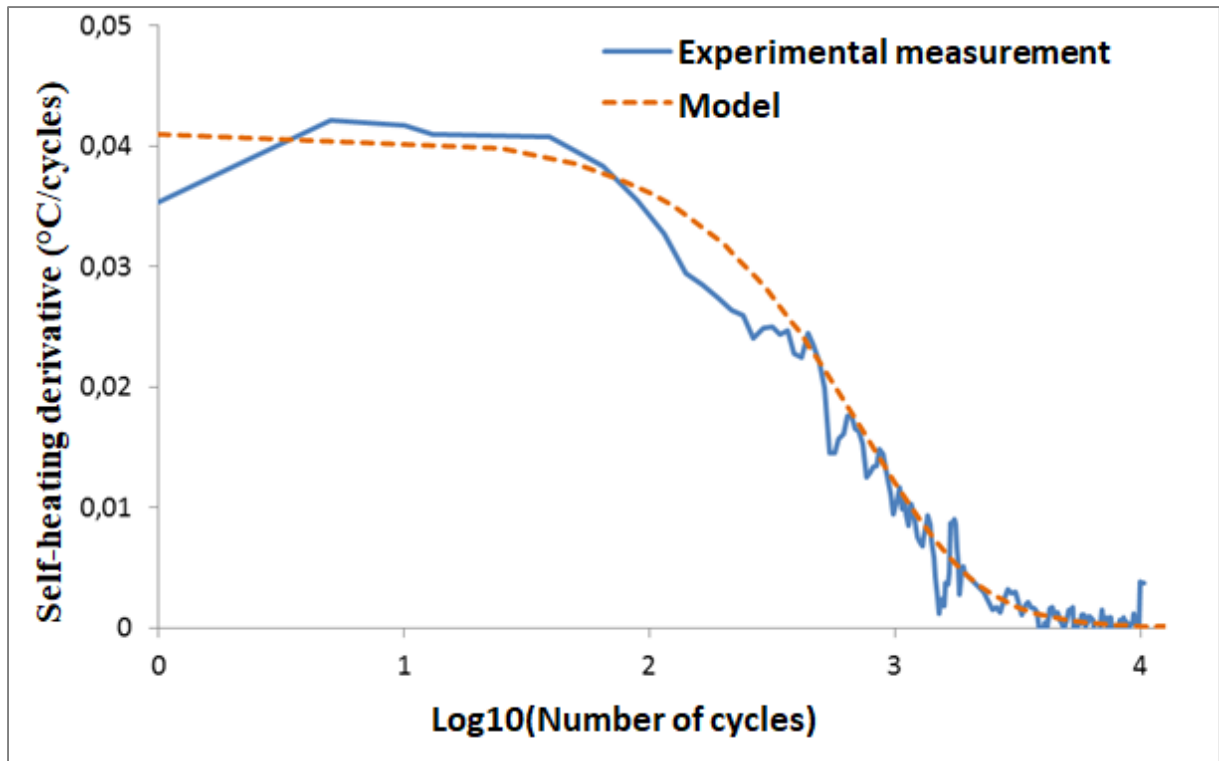


Figure 8 – Evolution of the self-heating derivative of the measured compared to the suggested model in the same conditions as on the figures 5 and 6 ($R=0.1$, Maximum load = 175N and fatigue life = 10^4 cycles).

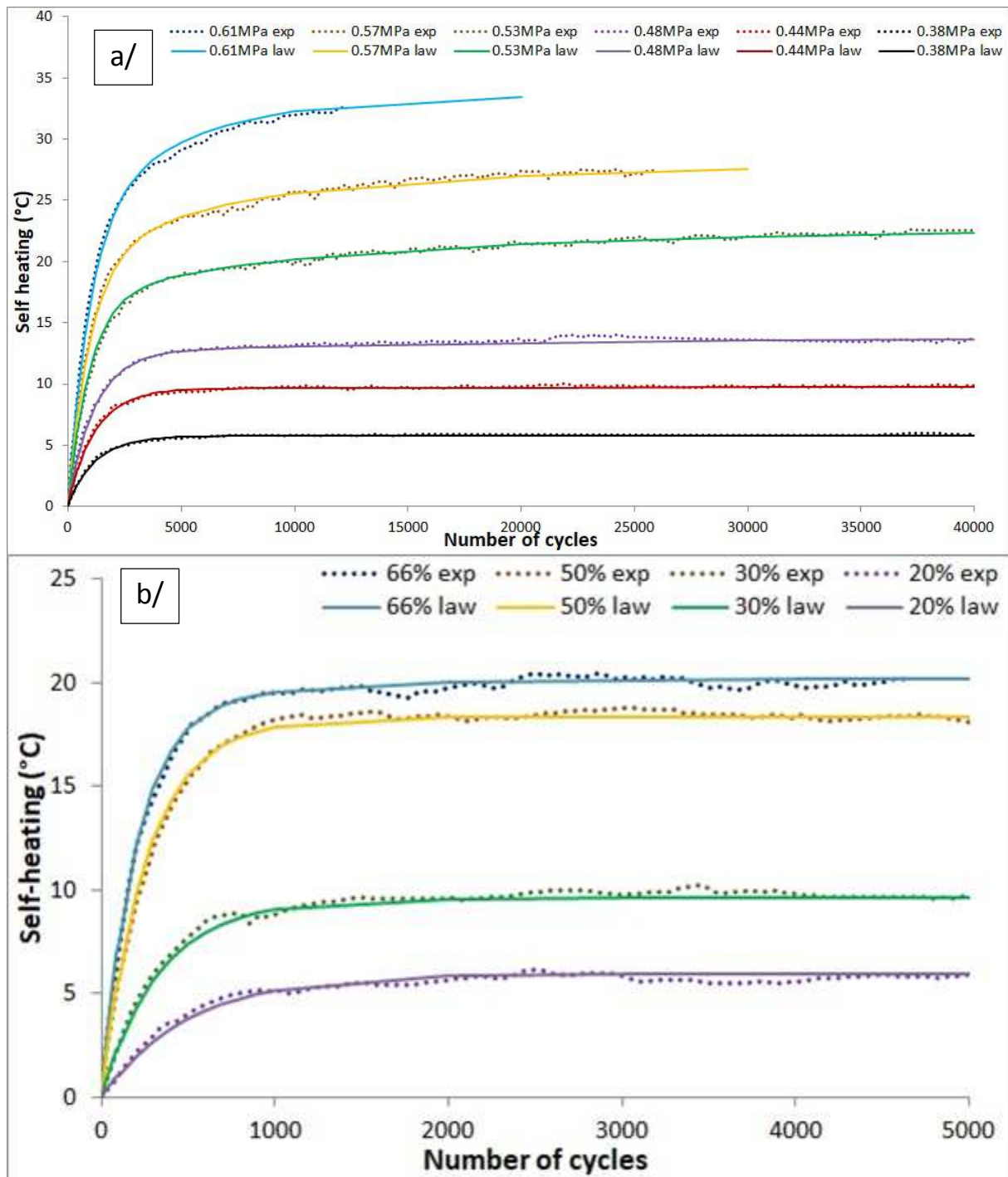


Figure 9 – Evolution of the self-heating measured experimentally (exp) compared to the proposed model (law). The results for the polychloroprene are shown on the figure a and for the natural rubber on the figure b. The tests are named with the amplitude loading applied.

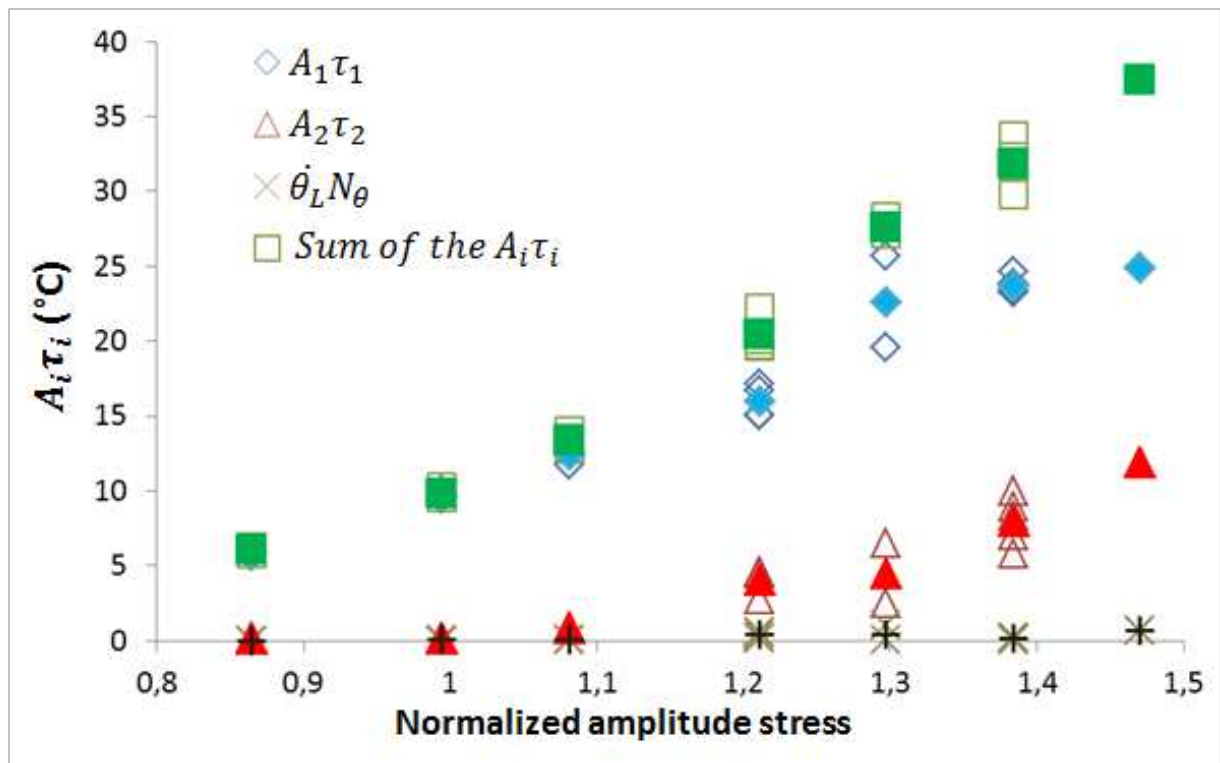


Figure 10 – $A_i \tau_i$ evolution and their sum versus the normalized amplitude stress at $R=0.1$ for the polychloroprene. The full figures stand for the averaged value for the given normalized amplitude stress. One hollow figure represents one test.

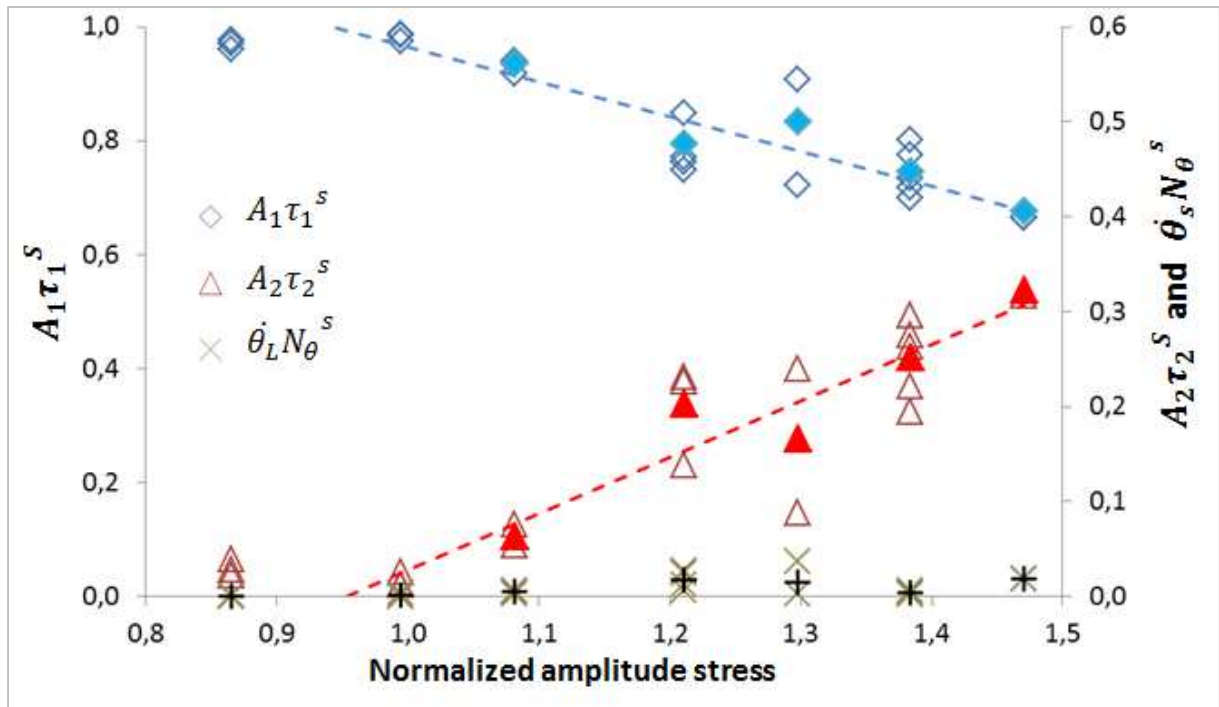


Figure 11 – $A_i\tau_i^s$ evolution versus the normalized amplitude stress at R=0.1 for the polychloroprene. The full figures stand for the averaged value for the given normalized amplitude stress. One hollow figure represents one test.

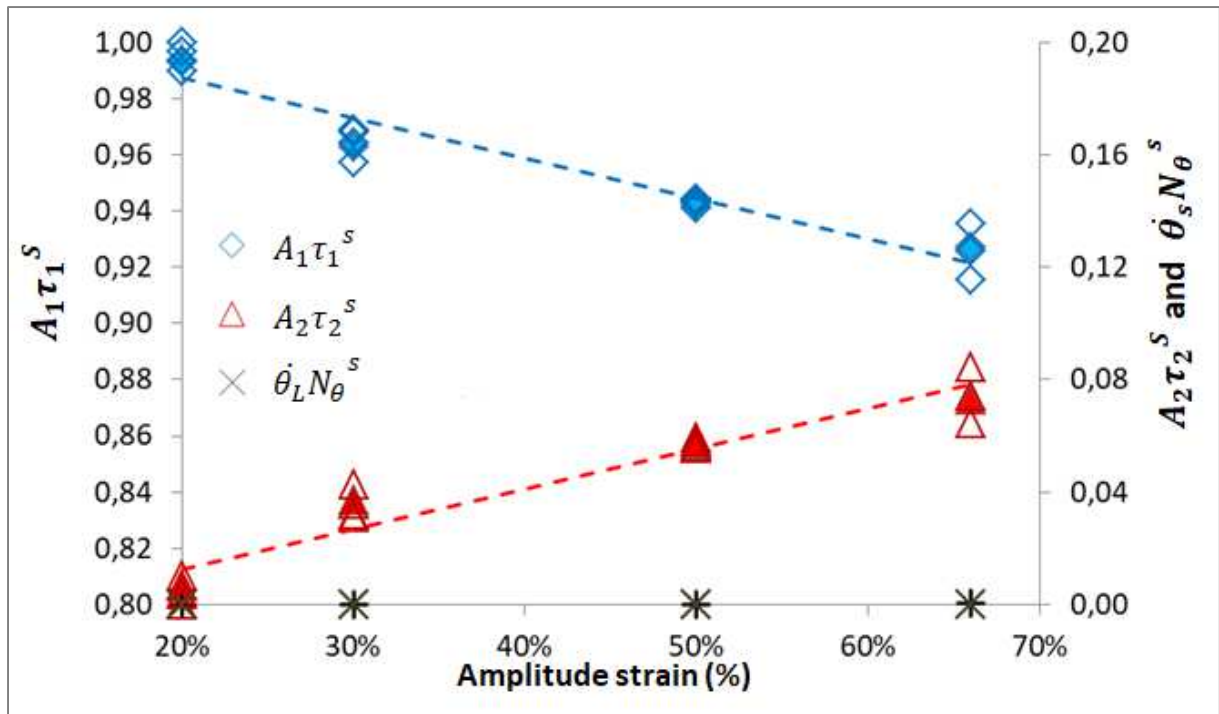


Figure 12 – $A_i\tau_i^s$ evolution versus the amplitude strain at $R=0.2$ for the natural rubber. The full figures stand for the averaged value for the given normalized amplitude stress. One hollow figure represents one test.

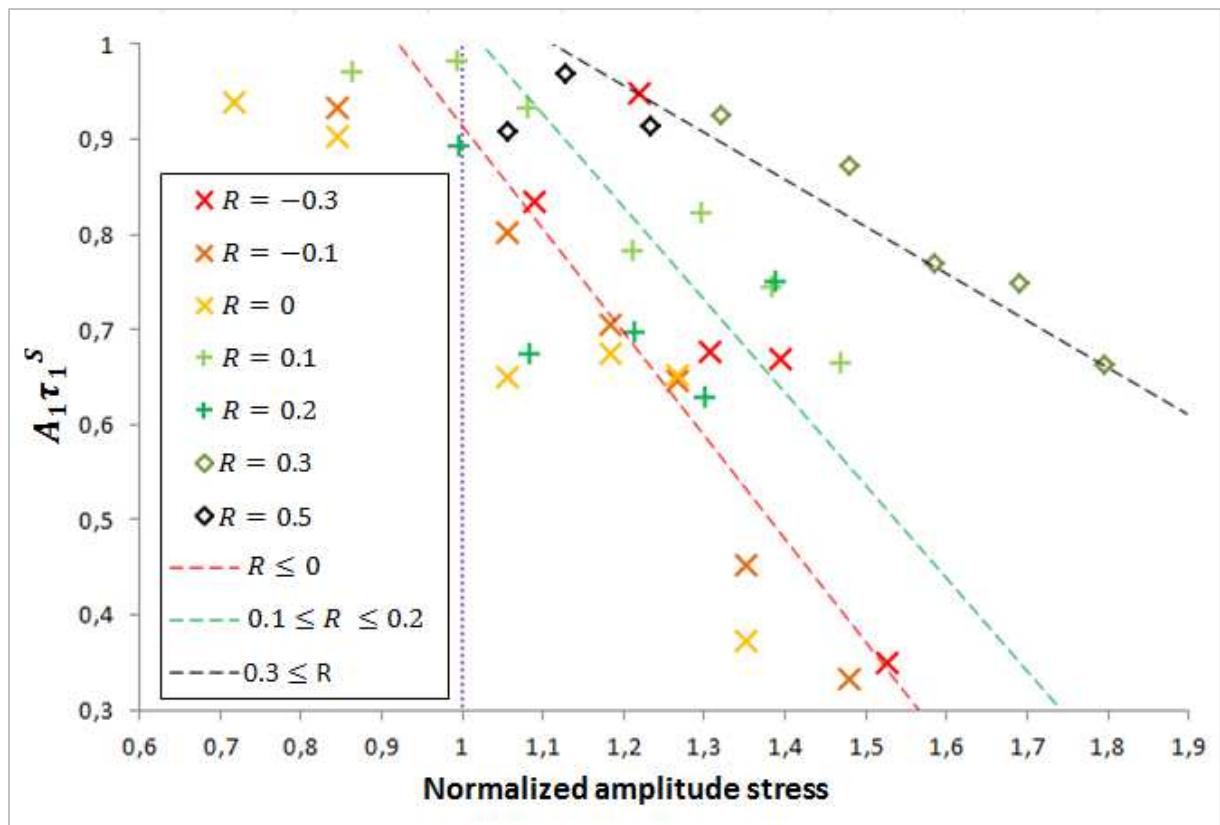


Figure 13 – Polychloroprene: evolution of averaged values of $A_1 \tau_1^s$ versus the normalized amplitude stress for each load ratio

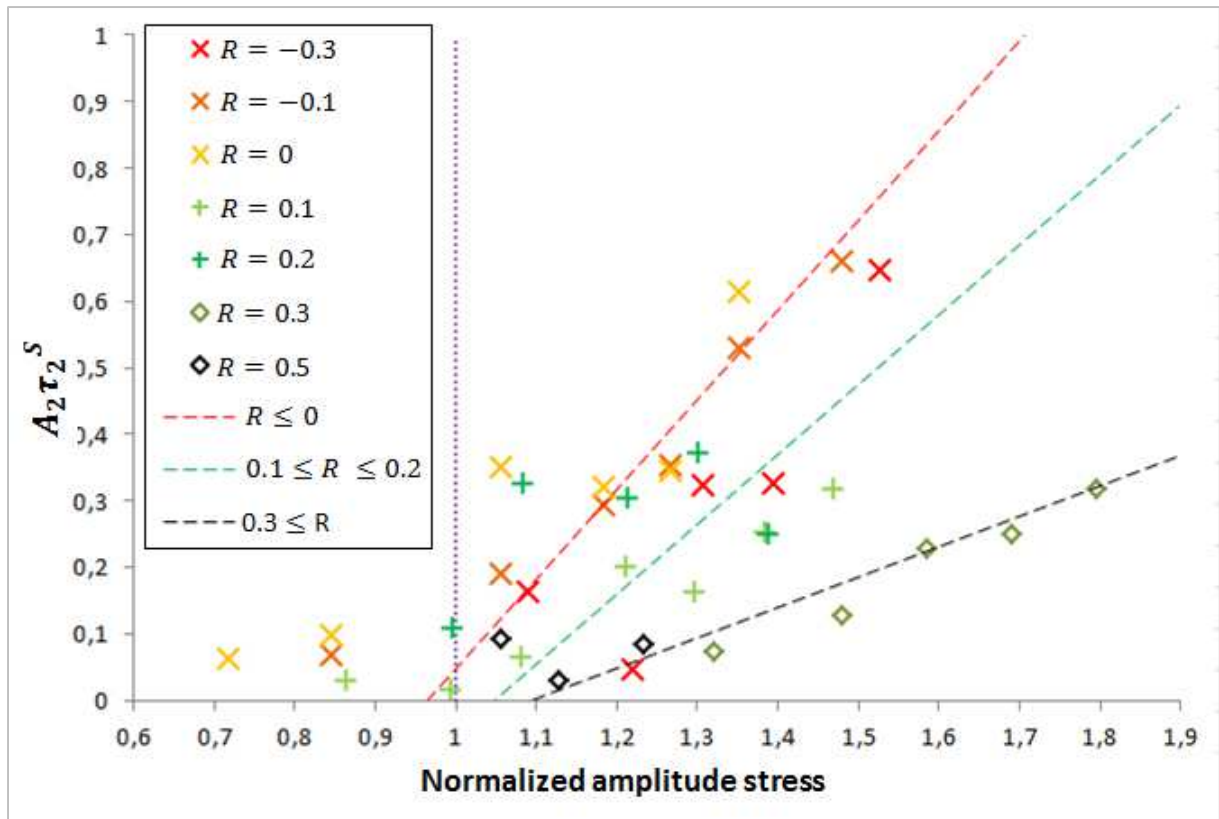


Figure 14 – Polychloroprene: evolution of averaged values of $A_2\tau_2^s$ versus the normalized amplitude stress for each load ratio

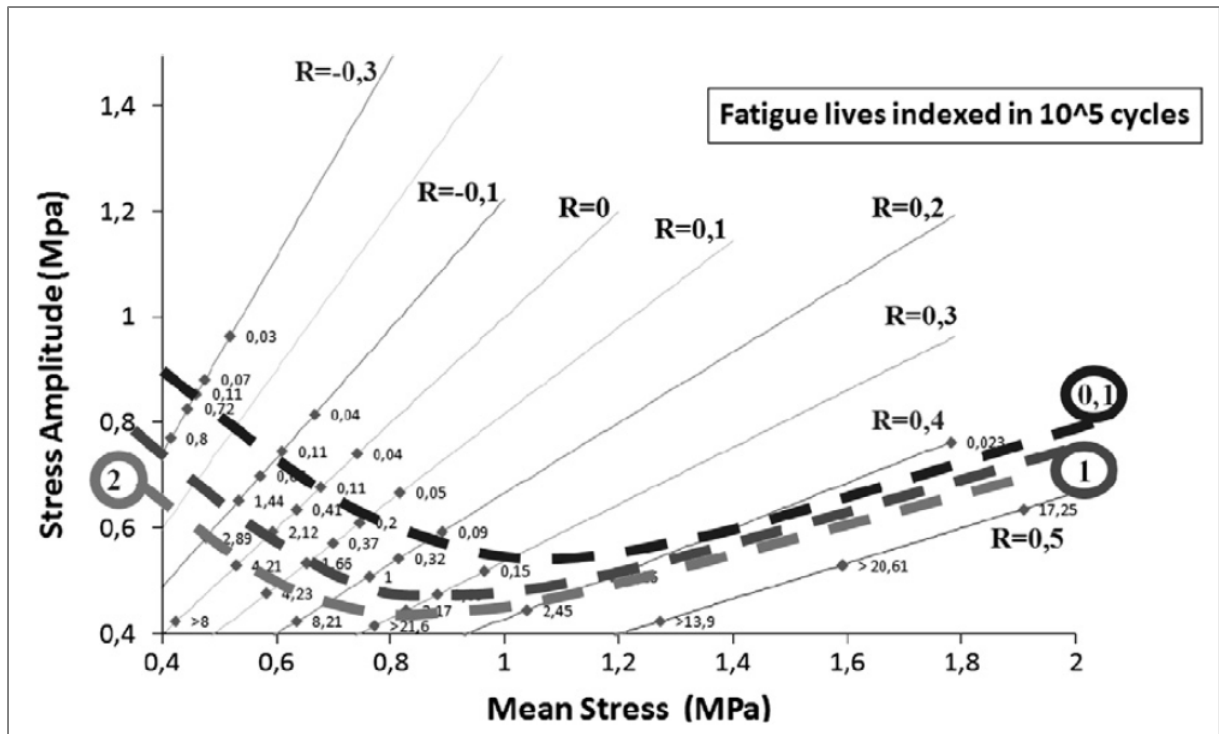


Figure 15 – Haigh diagram of a polychloroprene rubber from a tension and load control fatigue campaign (from [Poisson et al. 2011])

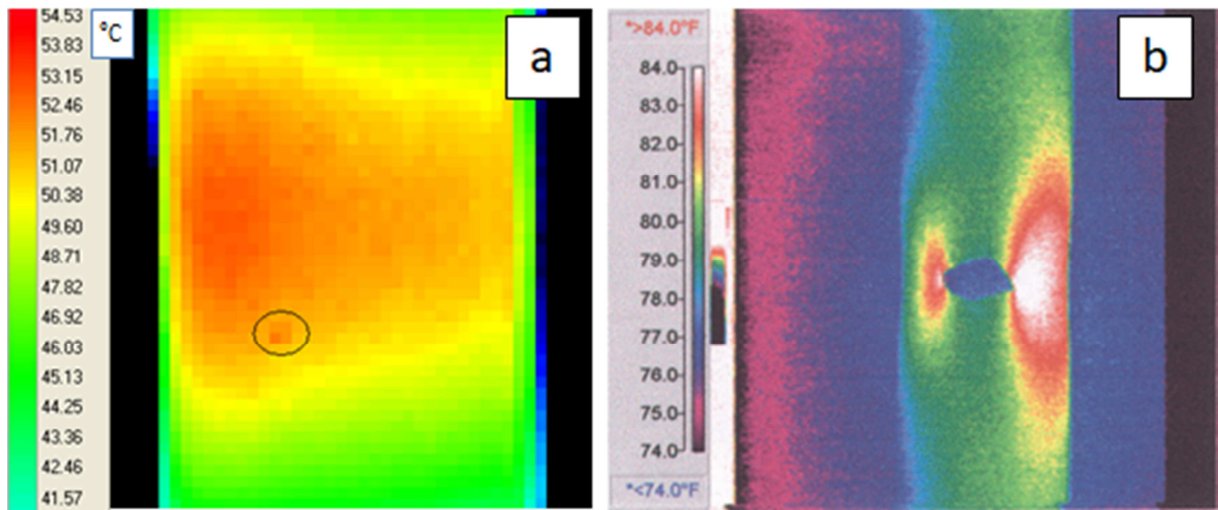


Figure 16 – Thermal images of samples taken around the middle of a fatigue test and exhibiting the influence of a crack on the thermal field. The material and sample showed are: a/ dumbbell in CR from this study and b/ ($66 \times 25,4 \times 1 \text{ mm}^3$) thin sample with an initial central cut in natural rubber [Kerchman et al. 2003].